Monthly Notices
of the
ROYAL ASTRONOMICAL SOCIETY

MNRAS **476,** 5535–5547 (2018)
Advance Access publication 2018 March 3

doi:10.1093/mnras/sty520

X-ray study of a sample of FR0 radio galaxies: unveiling the nature of the central engine

E. Torresi,[1,2]★ P. Grandi,[2] A. Capetti,[3] R. D. Baldi[4] and G. Giovannini[1,5]

[1]*Dipartimento di Astronomia, Università di Bologna, Via Gobetti 93/2, I-40129 Bologna, Italy*
[2]*INAF – OAS Bologna, Area della Ricerca CNR, Via Gobetti 101, I-40129 Bologna, Italy*
[3]*INAF – Osservatorio Astrofisico di Torino, Strada Osservatorio 20, I-10025 Pino Torinese, Italy*
[4]*Department of Physics and Astronomy, The University of Southampton, Southampton SO17 1BJ, UK*
[5]*INAF – IRA Bologna, Via Gobetti 101, I-40129 Bologna, Italy*

Accepted 2018 February 22. Received 2018 February 21; in original form 2017 July 4

ABSTRACT

Fanaroff–Riley type 0 radio galaxies (FR0s) are compact radio sources that represent the bulk of the radio-loud active galactic nuclei (AGN) population, but they are still poorly understood. Pilot studies on these sources have been already performed at radio and optical wavelengths: here we present the first X-ray study of a sample of 19 FR0 radio galaxies selected from the Sloan Digital Sky Survey/NRAO VLA Sky Survey/Faint Images of the Radio Sky at Twenty-cm sample of Best & Heckman, with redshift $\leq$0.15, radio size $\leq$10 kpc, and optically classified as low-excitation galaxies. The X-ray spectra are modelled with a power-law component absorbed by Galactic column density with, in some cases, a contribution from thermal extended gas. The X-ray photons are likely produced by the jet as attested by the observed correlation between X-ray (2–10 keV) and radio (5 GHz) luminosities, similar to Fanaroff–Riley type I radio galaxies (FRIs). The estimated Eddington-scaled luminosities indicate a low accretion rate. Overall, we find that the X-ray properties of FR0s are indistinguishable from those of FRIs, thus adding another similarity between AGN associated with compact and extended radio sources. A comparison between FR0s and low-luminosity BL Lacs rules out important beaming effects in the X-ray emission of the compact radio galaxies. FR0s have different X-ray properties with respect to young radio sources (e.g. gigahertz-peaked spectrum/compact steep spectrum sources), generally characterized by higher X-ray luminosities and more complex spectra. In conclusion, the paucity of extended radio emission in FR0s is probably related to the intrinsic properties of their jets that prevent the formation of extended structures, and/or to intermittent activity of their engines.

Key words: galaxies: active – galaxies: jets – X-rays: galaxies.

1 INTRODUCTION

The recent wide field surveys performed in the optical and radio bands (e.g. SDSS[1] and FIRST[2]) showed that the population of radio sources associated with active galactic nuclei (AGN) is dominated by objects in which the radio emission is unresolved or barely resolved in the FIRST images (e.g. Best et al. 2005; Baldi & Capetti 2010; Baldi, Capetti & Massaro 2018a): this implies that they have typical sizes of less than ∼10 kpc. In contrast, radio galaxies selected by high flux limited low-frequency surveys such as the 3C (Edge et al. 1959), the 3CR (Bennett 1962), the 4C (Pilkington & Scott 1965), and the B2 (Colla et al. 1975; Fanti et al. 1978) often extend to hundreds of kpc [Fanaroff–Riley type I (FRI)/Fanaroff–Riley type II (FRII) Fanaroff & Riley 1974] and appear resolved at the angular resolution provided by FIRST. Baldi & Capetti (2010) and Baldi et al. (2018a) showed that the radio galaxies selected in the local Universe at 1.4 GHz, with similar bolometric luminosities, span in a broad distribution of radio luminosities and sizes, from compact to resolved with clear extended radio emission. It is important to note that a clear dichotomy is not present among sources selected from classical low-frequency radio catalogues (B2, 3C, and 4C) and radio galaxies selected in the local Universe by surveys as the FIRST.

The lack of a clear difference in luminosity and size distribution requires to adopt an arbitrary angular size threshold, which furthermore corresponds to a different physical scale depending on distance. Therefore, a precise definition of the population of

★E-mail: torresi@iasfbo.inaf.it
[1] Sloan Digital Sky Survey (York et al. 2000).
[2] Faint Images of the Radio Sky at Twenty-cm survey (Becker, White & Helfand 1995; Helfand, White & Becker 2015).

compact radio sources suffers from several observational difficulties, mainly because they are selected from surveys (e.g. FIRST, NVSS[3] and AT20G[4]) limited in flux, resolution, and sensitivity.

Ghisellini (2011) first described the compact sources studied by Baldi & Capetti (2009, 2010) as Fanaroff–Riley type 0 radio galaxies (FR0s). The FR0 nomenclature was then followed by Sadler et al. (2014) 'as a convenient way of linking the compact radio sources seen in nearby galaxies into the canonical Fanaroff–Riley classification scheme.; However, Sadler et al. found a more diversified population, e.g. with significant contribution of high-excitation galaxies (HEGs), with respect to Baldi & Capetti (2010). These differences are likely related to a substantial distinction in the luminosity functions of the two samples considered: the Sadler et al. sources extend to a radio power ∼100 times higher at a radio frequency 10 times higher than the sample selected by Baldi & Capetti.

It is also clear that compact radio sources are a very heterogeneous population and they can be produced by AGN with widely different multiwavelength properties. For example, although most of them are radio-loud AGN, radio-quiet galaxies often show compact radio cores sometimes associated with pc/kpc scale emission (Ulvestad & Ho 2001; Nagar, Falcke & Wilson 2005; Baldi et al. 2018b). Furthermore, the properties of their hosts and nuclei differ depending on the frequency and flux threshold at which they are selected.

Considering the difficulties in univocally defining the class described above, Baldi & Capetti (2010) suggested to restrict the FR0 definition to a subpopulation of compact radio sources whose compactness is not due to relativistic effects and which do not follow the correlation between total and core radio power of classical FRI and FRII sources (Giovannini et al. 1988). Indeed, a source property useful to try a comparison and to select different populations with different properties could be the core dominance. Giovannini et al. (1988) discussed the core dominance properties for all sources from the 3CR and B2 catalogues with the only selection effect on the declination and galactic latitude. A clear correlation between the core and total radio power was found useful to constrain the source orientation and jet velocity. The best-fitting linear regression of $\log P_c$ versus $\log P_t$ gives (see Giovannini et al. 2001)

$$\log P_c = (7.6 \pm 1.1) + (0.62 \pm 0.04) \log P_t, \quad (1)$$

where P_c is the core radio power at 5 GHz and P_t is the total radio power at 408 MHz.

In a pilot program of high-resolution (∼0.2 arcsec) radio imaging of a small sample of compact sources, Baldi, Capetti & Giovannini (2015, hereafter B15) defined as genuine FR0 those sources that appear unresolved, or slightly resolved, on a scale of 1–3 kpc in the radio maps, that are located in red massive ($\sim 10^{11}$ $M_\odot$) early-type galaxies with high black hole masses ($M_{BH} \geq 10^8$ $M_\odot$) and that are spectroscopically classified in the optical as low-excitation galaxies (LEGs).[5] The sources of the B15 sample are highly core dominated, since most of the emission detected at 5 arcsec (FIRST resolution) is included within a compact region unresolved at 45 arcsec (NVSS resolution): this turns out in a core dominance higher by factor of ∼30 for FR0s with respect to FRIs of the 3CR catalogue.

Line luminosity is a robust proxy of the radiative power of the AGN and, at least for the sources with similar multiwavelength properties, of the accretion rate. At a given line luminosity, FR0s are ∼100 less luminous than FRIs in total radio power. Therefore, the compact radio galaxies studied by B15 are not simply unresolved sources, but they show a genuine lack of extended radio emission at large scales. Possible explanations have been proposed, such as (i) FR0s could be short-lived and/or recurrent episodes of AGN activity, not long enough for radio jets to develop at large scales (Sadler et al. 2014; Sadler 2016), or (ii) FR0s produce slow jets experiencing instabilities and entrainment in the dense interstellar medium of the host galaxy corona that causes their premature disruption (Bodo et al. 2013; B15; Baldi et al. 2018a).

In this paper we present the first systematic X-ray study of a sample of FR0 radio galaxies. Since the radio selection of compact radio galaxies carried out by Baldi & Capetti (2010) and B15 turns out to correspond to an optical selection, we adopt these radio and spectrophotometric characteristics to define our FR0 class of low-excitation radio galaxies. This classification differs from the other FR classes, not only for the radio morphology but also for specific spectrophotometric characteristics. The key aim of our work is to investigate the central regions of FR0s through X-rays in an effort to shed light on the nature of their central engine. A comparison with the radio, optical, and X-ray properties of the FRI radio galaxies is also pursued to further explore differences/similarities between these two classes of sources. Since the FR0/FRI comparison is one of the main drivers of the present study, this motivates our selection of only LEG spectroscopic types. Furthermore, this stricter definition of FR0 enables us to restrict on a more homogeneous population of compact sources, avoiding confusion with e.g. Seyfert-like objects or gigahertz-peaked spectrum (GPS)/compact steep spectrum (CSS) sources (see Section 4.3). Data were taken from the public archives of the X-ray satellites currently on-flight (e.g. *XMM–Newton*, *Chandra*, and *Swift*). Most of the X-ray data of our sample are unpublished.

Incidentally, we note that very recently a FR0 radio galaxy, i.e. Tol 1326−379, has been associated for the first time with a γ-ray source (Grandi, Capetti & Baldi 2016). Tol 1326−379 shows a GeV luminosity typical of FRIs but with a steeper γ-ray spectrum that can be related to intrinsic jet properties or to a different viewing angle. For this source, a *Swift* Target of Opportunity (ToO) observation was performed during the writing of the paper.

The paper is organized as follows. In Section 2 we define the sample. In Section 3 we describe the observations, data reduction, and spectral analysis, while the results are discussed in Section 4. Notes on single sources and details of the X-ray analysis are reported in Appendix A. The multiwavelength properties of the FRI comparative sample are listed in Appendix B. Throughout the paper we use the following cosmological parameters: $H_0 = 70\,\mathrm{km^{-1}\,s^{-1}\,Mpc^{-1}}$, $\Omega_m = 0.3$, $\Omega_\lambda = 0.7$ (Spergel et al. 2007).

2 SAMPLE SELECTION

In order to build our sample of FR0 sources we took at first the SDSS/NVSS/FIRST sample of radio galaxies by Best & Heckman

[3] National Radio Astronomy Observatory (NRAO) Very Large Array (VLA) Sky Survey (Condon et al. 1998).

[4] The Australia Telescope 20 GHz survey (Murphy et al. 2010).

[5] LEGs have generally weaker [O III] line emission with respect to HEGs that show [O III]/Hα > 0.2 and equivalent width of [O III] > 3 Å (Laing et al. 1994; Jackson & Rawlings 1997). More recent definitions have been provided by Kewley et al. (2006) on the basis of the $L_{[O\,III]}/\sigma^4$ quantity and Buttiglione et al. (2010) on the basis of the excitation index (EI) defined as EI = log[O III]/Hβ − 1/3(log[N II]/Hα + log [S II]/Hα + log [O I]/Hα). In particular, LEG sources are characterized by EI ≤ 0.95.

Table 1. Log of the observations of the FR0 sample.

SDSS name	Telescope	ObsID	Exposure (ks)	Offset (arcmin)
J004150.47−091811.2	*Chandra*	15173	42.5	3.4
J010101.12−002444.4[a]	*Chandra*	8259	16.8	0.0
J011515.78+001248.4[a]	*XMM*	0404410201	54.0	0.095
J015127.10−083019.3	*Swift*	00036976004	5.6	0.894
J080624.94+172503.7	*Swift*	00085577001	1.3	0.337
J092405.30+141021.5	*Chandra*	11734	30.1	0.0
J093346.08+100909.0	*Swift*	00036989002	12.2	1.867
J094319.15+361452.1	*Swift*	00036997001	5.4	3.437
J104028.37+091057.1	*XMM*	0038540401	24.0	0.003
J114232.84+262919.9	*XMM*	0556560101	32.9	13.7
J115954.66+302726.9	*Swift*	00090129001	3.4	2.803
J122206.54+134455.9	*Swift*	00083911002	1.3	7.641
J125431.43+262040.6	*Chandra*	3074	5.8	2.0
Tol 1326−379	*Swift*	00034308001	4.3	0.0
J135908.74+280121.3	*Chandra*	12283	10.1	3.1
J153901.66+353046.0	*Swift*	00090113002	2.8	0.96
J160426.51+174431.1	*Chandra*	4996	22.1	2.5
J171522.97+572440.2	*Chandra*	4194	47.9	0.0
J235744.10−001029.9[a, b]	*XMM*	–	–	–

Notes. [a]The source is already present in the FR0 sample of B15.
[b]This source is part of the Third *XMM–Newton* Serendipitous Source Catalog-Sixth Data Release (3*XMM*-DR6; Rosen et al. 2016).

(2012)[6] and we applied the criteria listed below, following the approach of B15. This guarantees that we are considering LEG compact sources:

(i) redshift $z \leq 0.15$;
(ii) compact in the FIRST images, corresponding to a radio size $\lesssim$10 kpc;
(iii) FIRST flux >30 mJy (to ensures a higher fraction of X-ray detected objects);
(iv) LEG optical classification.

We obtained a list of 73 objects from which we excluded the four sources classified as low-luminosity BL Lacs (Capetti & Raiteri 2015). We performed a search for X-ray observations of the remaining 69 sources available in the public archives of the X-ray satellites currently on-flight[7] and found 15 objects. Some sources are the target of the X-ray pointing, some others were serendipitous sources in the field of other targets. In order to enlarge the sample, we also included two FR0s already presented in B15 having public X-ray observations. These sources were not included in our starting sample since they have FIRST fluxes ∼10 mJy. Finally, during the writing of the paper Tol 1326−379, the first FR0 detected in γ-rays by the *Fermi* satellite (Grandi et al. 2016), was observed by *Swift* as a ToO and therefore it is considered in this work. The entire sample of FR0s studied here is reported in Table 1.

Fig. 1 shows the location of our 19 FR0s in the FIRST versus [O III] diagram adapted from B15. FR0s and 3CR/FRIs share the same range in $L_{[O\,III]}$, but FR0s have lower radio luminosities: this strong deficit in total radio emission places FR0s to the left of 3CR/FRIs (B15), confirming that our selection criteria are valid. Even considering low-luminosity radio galaxies such as FRICAT sources (Capetti, Massaro & Baldi 2017), FR0s still occupy the left-hand side of the plot (see fig. 6 of Baldi et al. 2018a) forming a continuous distribution from FR0 to sFRICAT, FRICAT, and 3CR/FRI sources. The low-luminosity BL Lacs of Capetti & Raiteri (2015; see also Baldi et al. 2018b) are also shown in Fig. 1 and have generally 1.4 GHz radio luminosities higher than FR0s (see Section 4.2). In the same plot also CoreG galaxies[8] are reported (for more details see Balmaverde & Capetti 2006; Baldi & Capetti 2009).

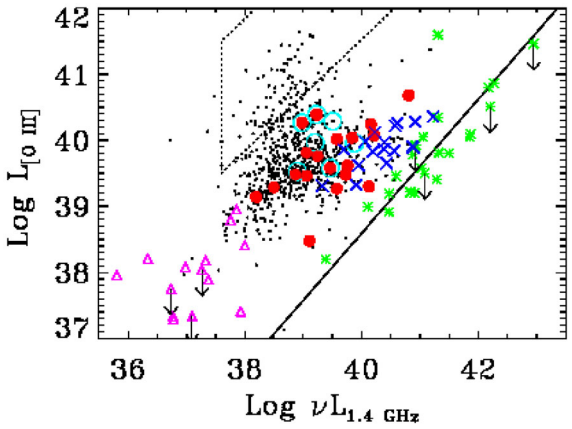

Figure 1. FIRST versus [O III] luminosities (both in erg s^{-1}) adapted from B15. Red points are the FR0s presented in this paper, while empty cyan circles are the FR0s of B15. The black dot points correspond to the SDSS/NVSS sample analysed by Baldi & Capetti (2010), the blue crosses are the low-luminosity BL Lacs studied by Capetti & Raiteri (2015), the empty pink triangles are the CoreG galaxies (Balmaverde & Capetti 2006), and the green stars are the FRIs of the 3CR sample. The dashed line marks the boundary of the location of Seyfert galaxies. The solid line represents the line-radio correlation followed by the 3CR/FRIs.

[6] Best & Heckman (2012) built a sample of 18 286 AGN by cross-correlating the Seventh Data Release of the SDSS with the NVSS and the FIRST. The sample is selected at a flux density level of 5 mJy.
[7] http://heasarc.gsfc.nasa.gov/cgi-bin/W3Browse/w3browse.pl

[8] CoreG galaxies are low-luminosity radio sources hosted by early-type galaxies and defined 'core' on the basis of the presence of a shallow core in their host surface brightness profile.

Table 2. Radio parameters: (1) source name; (2) flux ratio between FIRST and NVSS fluxes; (3) radio spectral index ($S_\nu \propto \nu^\alpha$) between 8.5 GHz (The Cosmic Lens All Sky Survey, CLASSSCAT; Browne et al. 2003; Myers et al. 2003) and 1.4 GHz (NVSS) otherwise specified in the notes; and (4) core dominance, R, defined as the ratio between 8.5 GHz (CLASSSCAT) and 1.4 GHz (NVSS) flux densities.

Source name (1)	$F_{\rm FIRST}/F_{\rm NVSS}$ (2)	$\alpha_{\rm r}$ (3)	$\log R$ (4)
J004150.47−09	0.74	-0.13^a	–
J010101.12−00	0.70	-0.45^b	-0.47^b
J011515.78+00	1.05	-0.04^b	-0.06^b
J015127.10−08	0.88	–	–
J080624.94+17	0.96	–	–
J092405.30+14	0.95	–	–
J093346.08+10	0.80	−0.47	−0.37
J094319.15+36	0.99	0.82	0.65
J104028.37+09	0.94	-0.63^a	–
J114232.84+26	0.94	0.11	0.09
J115954.66+30	1.06	−0.01	−0.01
J122206.54+13	0.99	0.28	0.22
J125431.43+26	0.98	−0.47	−0.37
Tol 1326−379	–	0.37^c	−0.42
J135908.74+28	1.12	−0.12	−0.09
J153901.66+35	0.92	−0.10	−0.08
J160426.51+17	0.75	0.15	0.12
J171522.97+57	0.86	−0.43	−0.34
J235744.10−00	0.65	-0.67^b	-0.58^b

Notes. [a]$\alpha_{\rm r}$ between 4.9 GHz (JVASPOL or PMN) and 1.4 GHz.
[b]Values of $\alpha_{\rm r}$ and R are from B15.
[c]The value of $\alpha_{\rm r}$ is from Grandi et al. (2016).

The radio properties of our sample meet the FR0 criteria discussed by B15. The sources generally show flat radio spectra and are compact. Indeed, as shown in Table 2, the ratios between the FIRST and NVSS fluxes at 1.4 GHz are around 1, indicating that the extended component in these sources is negligible. The core dominance R[9] is on average ∼30 times higher than 3CR/FRIs and overlaps with the FR0 values of B15 (Fig. 2). The paucity of information at radio frequencies higher than 1.4 GHz for the FRICAT sources prevents us from comparing their core dominance with our X-ray sample of FR0s. Finally, the radio spectral indices measured between 8.5 GHz (4.9 GHz) and 1.4 GHz are generally flat with a median value $\alpha_{\rm r} = -0.04$ (see Table 2 for more details).

3 X-RAY OBSERVATIONS AND ANALYSIS

3.1 Data reduction

Data were collected from different X-ray satellites. In particular, seven sources were observed with *Chandra*, four with *XMM–Newton*, and eight with *Swift*/X-Ray Telescope (XRT). The observation log is in Table 1. Several FR0 sources are not the primary target of the observation but are in the field of view of the pointing. The offset, i.e. the distance from the centre of the source cone,[10] is also reported in Table 1. When more than one observation was available, we chose the one with the smaller offset or the longer exposure. We reduced data for all the sources but one, i.e. J235744.10−00,

[9] R is defined as the ratio between 8.5 GHz (CLASSSCAT; Browne et al. 2003; Myers et al. 2003) and 1.4 GHz (NVSS) flux densities.
[10] See also https://heasarc.gsfc.nasa.gov/W3Browse/w3browse-help.html#distance_from_center.

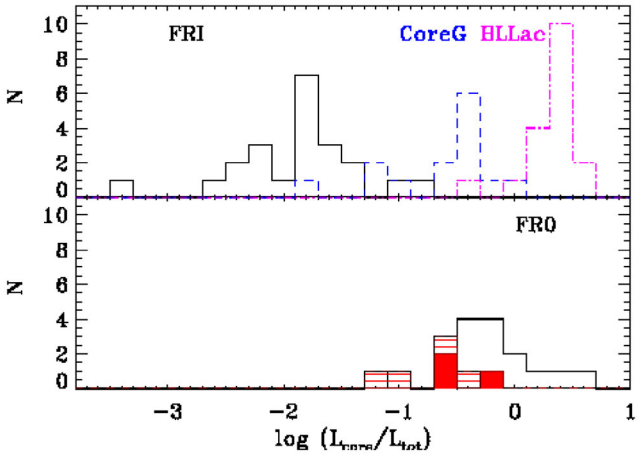

Figure 2. Histograms of the core dominance (adapted from B15) for – upper panel – 3CR/FRIs (black solid line), CoreG (blue dashed line), and low-luminosity BL Lacs (magenta dot–dashed line). Lower panel – FR0s of B15 (red ticked line) and our sample of FR0s (black solid line). The red filled histograms are the sources in common with B15.

since it is part of the Third *XMM–Newton* Serendipitous Source Catalog-Sixth Data Release (3*XMM*-DR6; Rosen et al. 2016).

All *Chandra* observations were performed using CCD, both Advanced CCD Imaging Spectrometer-S array (ACIS-S) and ACIS-I array. Data were reprocessed using CIAO version 4.7 with calibration data base CALDB version 4.6.9 and applying standard procedures. Table A1 reports the extraction regions chosen for the nuclear and background spectra of each source. Data were then grouped to a minimum of 15 counts bin^{-1} over the energy range 0.5–7 keV. None of the seven sources pointed by *Chandra* are affected by pile-up.

For the *XMM–Newton* observations we reduced and analysed data from the European Photon Imaging Camera (EPIC)-pn camera using SAS version 14.0 and the latest calibration files. Periods of high particle background were screened by computing light curves above 10 keV. Extraction regions for the source and background spectra are reported in Table A1. Data were then grouped to a minimum of 15 counts bin^{-1} over the energy range 0.5–10 keV for two out of the three sources. For the source J235744.10−00 the 0.2–12 keV flux was directly taken from the 3*XMM*-DR6 catalogue, and extrapolated to 2–10 keV assuming the same spectral slope adopted in the catalogue.

Swift/XRT data were reduced using the online data analysis tool provided by the ASI Space Science Data Center (SSDC).[11] The only exception is Tol 1326−379 that was observed as a ToO during the writing of the paper and the data were processed and analysed using standard XRT tools (XRTPIPELINE v.0.13.2 and CALDB v.1.0.2). Source spectra for each observation were extracted from a circular region of 20 arcsec radius, while the background was taken from an annulus with an inner radius of 40 arcsec and outer radius of 80 arcsec. Spectra were grouped to a minimum of 5 (or 3) counts bin^{-1} in the energy range 0.5–10 keV. In the case of the source J153901.66+35 no grouping was applied.

3.2 Imaging analysis

The inspection of the X-ray images indicates that six sources are in a dense environment (Fig. 3). Four lie at the outskirts of a cluster

[11] http://swift.asdc.asi.it/

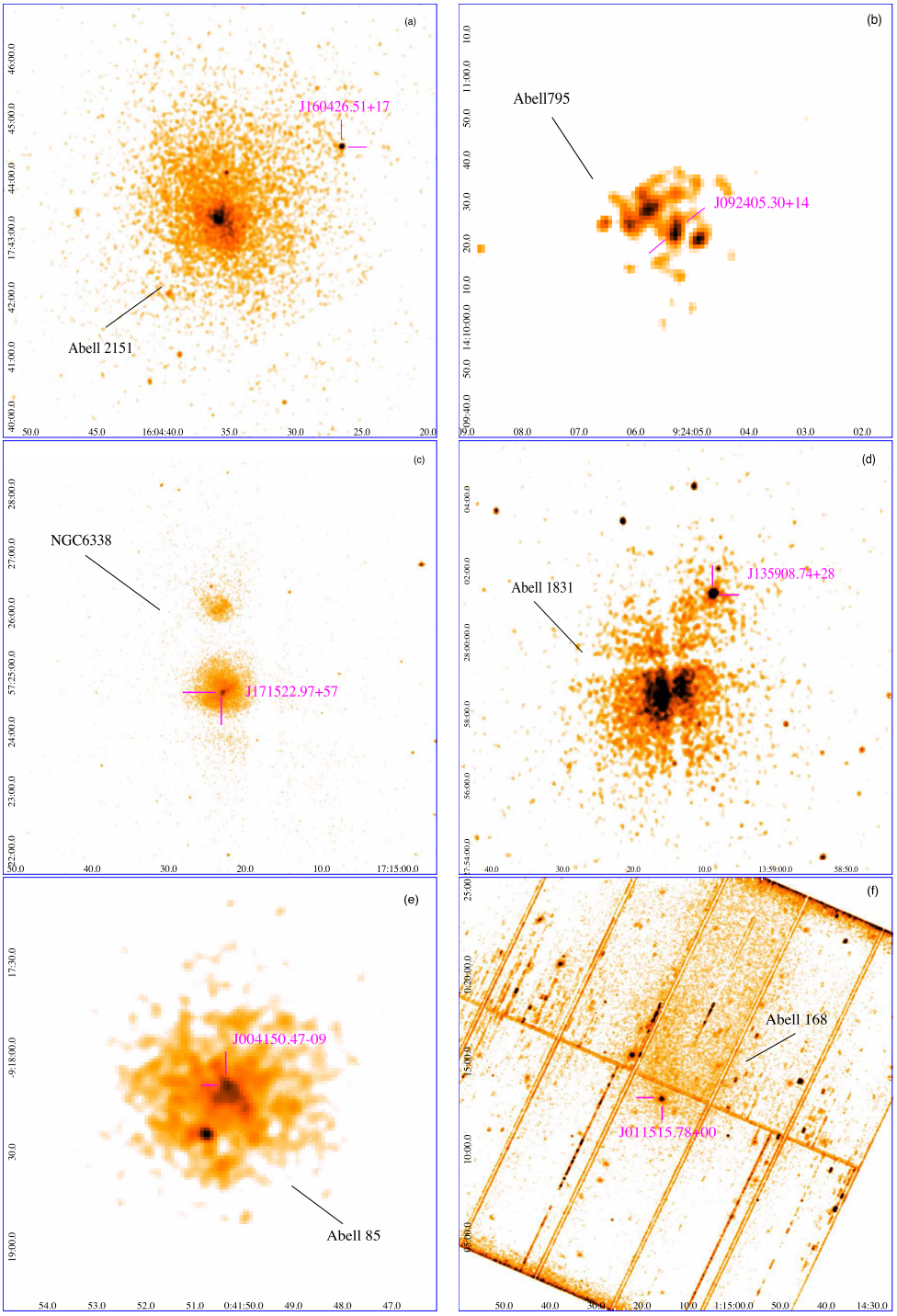

Figure 3. Images of the clusters found in the X-ray band. Panels (a)–(d): *Chandra* 0.3–7 keV images of the sources J160426.51+17, J092405.30+14, J171522.97+57, and J135908.74+28. The FR0 is labelled in magenta, while the name of the cluster is in black. Panel (e): *Chandra* 3–7 keV image of the source J004150.47−09. Panel (f): *XMM–Newton*/pn image of the source J011515.78+00. All images have been smoothed with a Gaussian with kernel radius 3.

of galaxies (i.e. J160426.51+17, J092405.30+14, J135908.74+28, and J011515.78+00), J004150.47−09 is located at the centre of the cluster Abell 85, and J171522.97+57 is the brightest member in a compact group of more than 13 galaxies (Pandge et al. 2012).

For the sources for which a clear extension cannot be confirmed by the X-ray images, information on the environment was checked in the literature (see Table 3). Other four sources were found in clusters or compact groups (CG), i.e. J093346.08+10, J122206.54+13, J080624.94+17, and J115954.66+30 (Owen, Ledlow & Keel 1995; Koester et al. 2007; Díaz-Giménez et al. 2012). In summary, we found that at least 50 per cent of the FR0s of our sample is in a dense environment. This value should be considered as a lower limit to the fraction of FR0s in dense environments in our sample since the analysis suffers from a bias due to the nature of the sample

Table 3. Main spectral parameters of the FR0 sample: (1) name of the source; (2) redshift; (3) best-fitting spectrum; (4) Galactic hydrogen column density; (5) power-law photon index; (6) temperature of the thermal component (APEC); (7) flux of the thermal component in the soft X-ray band (0.5–5 keV) corrected for Galactic absorption; (8) flux of the non-thermal component in the 2–10 keV band corrected for Galactic absorption; (9) χ^2/degrees of freedom reported when the grouping was ≥15, when the grouping was <15 the C-statistics was applied; (10) type of environment; and (11) references for the environment.

Source name	z	Best spectrum	$N_{H,Gal}$ (atoms cm^{-2})	Γ	kT (keV)	$F_{th,0.5-5\,keV}$ (erg cm^{-2} s^{-1})	$F_{nuc,2-10\,keV}$ (erg cm^{-2} s^{-1})	χ^2/dof	Environment	Reference[d]
(1)	(2)	(3)	(4)	(5)	(6)	(7)	(8)	(9)	(10)	(11)
J004150.47−09	0.055	PL	2.8×10^{20}	2.0 (fix)	–	–	$(4.5^{+2.9}_{-2.8}) \times 10^{-14}$	1.4/3	Cluster	1
J010101.12−00	0.097	PL	3.2×10^{20}	2.0 (fix)	–	–	$<6.6 \times 10^{-15}$	–	?	–
J011515.78+00	0.045	APEC+PL	3.0×10^{20}	2.0 ± 0.2	0.8 ± 0.1	$(1.5 \pm 0.4) \times 10^{-14}$	$(2.9^{+0.5}_{-0.4}) \times 10^{-14}$	66/63	Cluster	1
J015127.10−08	0.018	APEC+PL	2.3×10^{20}	2.0 (fix)	$0.2^{+0.3}_{-0.1}$	$(1.4^{+113}_{-1.3}) \times 10^{-13}$	$<4.2 \times 10^{-14}$	–	?	–
J080624.94+17	0.104	PL	3.3×10^{20}	2.0 (fix)	–	–	$(3.2^{+1.7}_{-1.4}) \times 10^{-13}$	–	Cluster	2
J092405.30+14	0.135	APEC+PL	3.3×10^{20}	1.8 ± 0.3	$1.3^{+1.4}_{-0.6}$	$(5.9^{+19}_{-5}) \times 10^{-15}$	$(3.2^{+1.1}_{-2.8}) \times 10^{-14}$	3/9	Cluster	1
J093346.08+10	0.011	APEC+PL	3.1×10^{20}	2.0(fix)	<0.35	$<1.2 \times 10^{-13}$	$(6.2^{+2.7}_{-2.1}) \times 10^{-14}$.	–	CG[c]	3
J094319.15+36	0.022	PL	1.1×10^{20}	2.3 ± 0.4	–	–	$(7.9^{+2.3}_{-2.0}) \times 10^{-14}$	–	?	–
J104028.37+09	0.019	PL	2.6×10^{20}	2.2 ± 0.4	–	–	$(1.2 \pm 0.2) \times 10^{-14}$	3/7	Isolated	4
J114232.84+26	0.03	APEC+PL	2.0×10^{20}	2.0 (fix)	$0.67^{+0.07}_{-0.06}$	$(4.5 \pm 0.1) \times 10^{-14}$	$<1.3 \times 10^{-14}$	-	CG[c]	3
J115954.66+30	0.106	PL	1.5×10^{20}	2.0 (fix)	–	–	$(4.9^{+4.9}_{-3.1}) \times 10^{-14}$	–	?	–
J122206.54+13	0.081	PL	3.5×10^{20}	2.0 (fix)	–	–	$(1.0^{+1.2}_{-0.7}) \times 10^{-13}$	–	Cluster	5
J125431.43+26	0.069	PL	7.5×10^{19}	1.9 ± 1.4	–	–	$(9.2^{+1.8}_{-1.6}) \times 10^{-14}$	4/5	?	–
Tol 1326−379	0.028	PL	5.5×10^{20}	1.3 ± 0.4	–	–	$(9.4^{+1.9}_{-3.1}) \times 10^{-13}$	–	?	–
J135908.74+28	0.073	APEC+PL	1.3×10^{20}	2.0 (fix)	0.24 (fix)[a]	$(1.9^{+0.8}_{-0.7}) \times 10^{-13}$	$(5.0^{+2.2}_{-2.3}) \times 10^{-14}$	0.5/2	Cluster	1
J153901.66+35	0.078	PL	1.8×10^{20}	2.0 (fix)	–	–	$(1.1^{+0.7}_{-1.0}) \times 10^{-13}$	–	?	–
J160426.51+17	0.041	PL	3.4×10^{20}	1.1 ± 0.3	–	–	$(1.5^{+0.5}_{-0.3}) \times 10^{-13}$	2.5/8	Cluster	1
J171522.97+57	0.027	APEC+PL	2.2×10^{20}	2.0 (fix)	1.1 ± 0.1[b]	$(1.2^{+0.4}_{-0.5}) \times 10^{-13}$	$<1.9 \times 10^{-14}$	70/53	CG[c]	1
J235744.10−00	0.076	PL	3.3×10^{20}	2.0 (fix)	–	–	$(9.7^{+7.9}_{-5.1}) \times 10^{-14}$	–	Isolated	6

Notes. [a]Because of the poor statistics of the fit this parameter is fixed to the best-fitting value.
[b]The abundance parameter is left free and reaches a value of Ab $= 0.3^{+0.3}_{-0.1}$.
[c]CG – compact group of galaxies.
[d]1 – this work; 2 – Koester et al. (2007); 3 – Díaz-Giménez et al. (2012); 4 – Colbert, Mulchaey & Zabludoff (2001); 5 – Owen et al. (1995); 6 – Prada et al. (2003).

mainly consisting of X-ray serendipitous sources. However, we are aware that strong conclusions on the environment of FR0 as a class cannot be drawn with the available data.

3.3 Spectral analysis

The spectral analysis was performed using the XSPEC version 12.9.0 package. We applied a χ^2 statistics to spectra binned to a minimum of at least 15 counts bin^{-1}. When the grouping was smaller a C-statistics was adopted. Errors are quoted at 90 per cent confidence for one interesting parameter ($\Delta\chi^2 = 2.71$). The summary of the best-fitting spectral results is reported in Table 3. Notes on single sources can be found in Appendix A.

Spectral fitting was performed in the energy range 0.5–7 keV (*Chandra*) and 0.5–10 keV (*XMM–Newton* and *Swift*). The X-ray luminosities presented throughout the paper are calculated in the 2–10 keV range in order to make a direct comparison with the literature. As a baseline model, we considered a power law convolved with the Galactic column density (Kalberla et al. 2005). In four out of six sources for which we could directly observe the cluster in the X-ray images (Fig. 3), residuals showed evidence for the presence of a soft component. Therefore we included a thermal model (APEC). A thermal component was also required in other three FR0s. The presence of a compact group was attested in J093346.08+10 and J115954.66+30 checking the literature. For the third one (i.e. J015127.10−08) no information on the environment was found. The nature of the soft X-ray emission is however uncertain. It could be due to an extended intergalactic medium (that cannot be revealed because of poor X-ray spatial resolution and/or short exposure time) or related to the hot corona typical of early-type galaxies (Fabbiano, Kim & Trinchieri 1992).

We could measure the power-law photon indices Γ for seven out of 18 objects. The spectral slopes are generally steep, with a mean value $\langle\Gamma\rangle = 1.9$ and a standard deviation of 0.3. When it was not possible to leave the photon index free, it was fixed to a value of 2. We checked whether different values of the photon index lead to significant changes in the estimate of the fluxes. We found that for Γ ranging between 1.5 and 2.5 the fluxes are consistent within the errors. In four cases the low statistics did not allow us to constrain the power-law component and to exclude the presence of thermal

emission, therefore we assumed a simple power law ($\Gamma = 2$ fixed) as the best-fitting model and we adopted the resulting 2–10 keV flux as upper limit for the nuclear component.

Generally, the X-ray spectra of our sample do not show evidence for intrinsic absorption. Indeed, the addition of an intrinsic absorber component does not improve significantly the fit. An upper limit to this component can be estimated only for three out of 18 sources (see Appendix A). Therefore, we tend to favour the scenario in which the circumnuclear environment of FR0 is depleted of cold matter, similarly to FRIs (Balmaverde, Capetti & Grandi 2006; Baldi & Capetti 2008, 2010; Hardcastle, Evans & Croston 2009).

The analysed FR0s have X-ray nuclear luminosities covering three orders of magnitude 10^{40-43} erg s^{-1}. The average value including the upper limits is $\langle \log L_X \rangle = 41.30$ (see Fig. 4, upper panel).

4 DISCUSSION

4.1 Compact versus extended low-excitation radio galaxies

FR0/LEGs and FRI/LEGs reside in similar galaxies and share similar nuclear optical properties (B15 and references therein). Given that low-ionization optical spectra can be also produced by shocks or old stellar population emission (Binette et al. 1994; Sarzi et al. 2010; Capetti & Baldi 2011; Balmaverde & Capetti 2015; Mingo et al. 2016), this X-ray study is a key tool to compare FR0 and FRI properties taking advantage of an energy band directly related to the nuclear emission processes.

We compared the X-ray luminosities of our sample to those of 35 FRI radio galaxies belonging to the 3CR/3CRR catalogues and having X-ray data available. The 2–10 keV luminosities of FRIs are from literature or obtained by a direct analysis of the data stored in the public archives (see Appendix B for details). Various samples of FRIs can be considered for the comparison with compact radio sources. For example the 3C sample includes ∼30 FRIs, the B2 sample is formed by ∼100 radio galaxies, about half of them being FRIs. The recent FRICAT catalogue is formed by 219 sources, selected from the SDSS/NVSS surveys, with a flux limit of 5 mJy at 1.4 GHz. However, the multiwavelength information is rather limited and, in particular, the coverage of X-ray observations is very small for all samples except for the 3C for which *Chandra* data are available for all sources up to $z = 1$ (Massaro et al. 2010, 2012, 2013). Being selected with a rather high flux threshold (9 Jy at 178 MHz), they represent the tip of the iceberg of the FRI population. While this means that the view of FRIs offered by the 3C sample is limited, they certainly provide us with a benchmark against which compare the properties of the compact radio sources.

The two distributions in Fig. 4 (upper panel) clearly overlap: the two samples test univariate program in the ASURV package (TWOST; Feigelson & Nelson 1985; Isobe, Feigelson & Nelson 1986) applied to the data (including upper limits) confirms their similarity ($P_{\rm ASURV} = 0.76$).[12] We assume that $P = 0.05$ is the probability threshold to rule out the hypothesis that the two samples are drawn from the same parent population. This result indicates a strong correspondence between the X-ray cores of low-excitation FR0 and FRI radio galaxies.[13]

[12] Probability value according to the Gehan's generalized Wilcoxon test.
[13] A similar result is obtained even excluding upper limits and applying a Kolmogorov–Smirnov test to the data ($P_{\rm KS} = 0.45$).

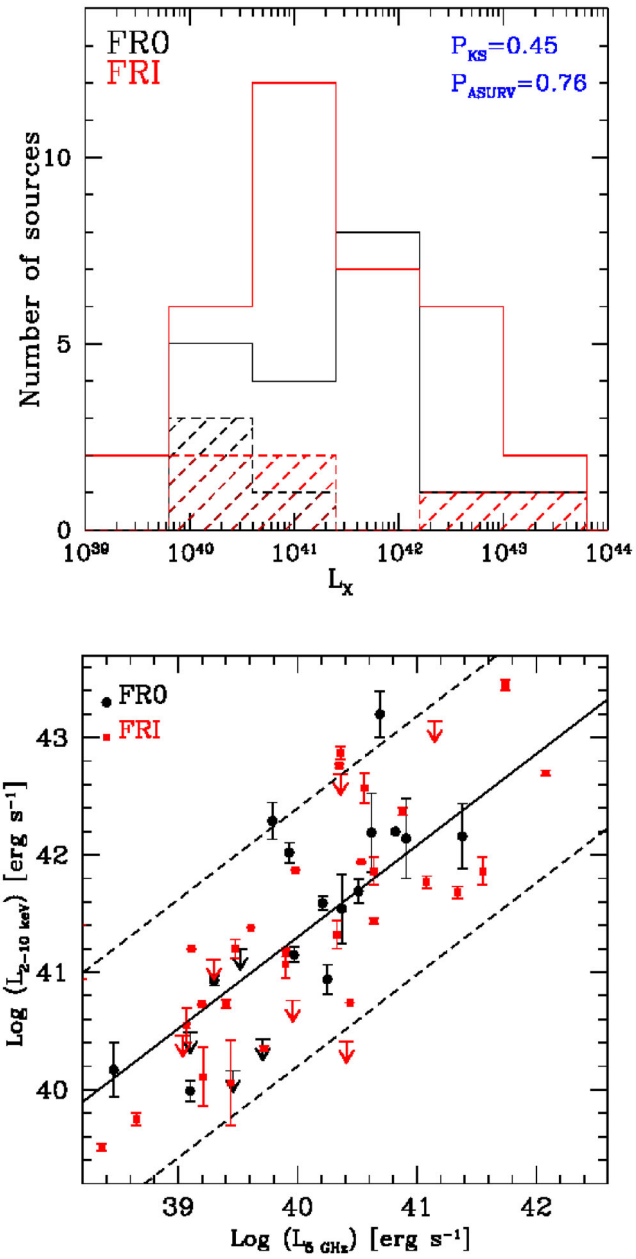

Figure 4. Upper panel: histogram of the X-ray luminosity for the FR0s of our sample (black solid line) and the comparative sample of FRIs (red solid line). No significant difference is observed between the two samples. The dashed histograms represent upper limits in each sample. In the plot the probabilities from the Kolmogorov–Smirnov test ($P_{\rm KS}$) and the TWOST test in ASURV ($P_{\rm ASURV}$) are also reported. Lower panel: 2–10 keV X-ray luminosity versus 5 GHz radio core luminosity for FR0s (black circles) and FRIs (red squares). Arrows indicate upper limits. The black solid line is the linear regression for the overall sample of FR0s and FRIs (excluding the upper limits): $\log L_X = (7.8 \pm 0.6) + (0.8 \pm 0.1) \log L_{5\,\rm GHz}$ (see also Hardcastle et al. 2009). The black dashed lines are the uncertainties on the slope.

This point is strengthened by Fig. 4 (lower panel) where the X-ray (2–10 keV) and radio core (5 GHz) luminosities of FR0s and FRIs are plotted together. Apart from the two objects having measurements at 4.9 GHz (see Table 2), the luminosities at 5 GHz of the compact sources were extrapolated from 1.4 GHz (FIRST) data considering the radio spectral slopes reported in Table 2. The core luminosities of the extended radio galaxies are from literature

(Hardcastle et al. 2009; Buttiglione et al. 2010, 2011). The two samples occupy the same area in the plot: the generalized Kendall's τ test (ASURV package; Isobe et al. 1986) gives a probability of correlation greater than 99.99 and 99.95 per cent for FRIs and FR0s (including upper limits), respectively.

We also tested the possible influence of redshift in driving this correlation estimating a partial rank coefficient.[14] The effect is negligible and the value of the correlation coefficient does not change significantly.

The correlation between $L_{\rm X}$ and $L_{5\,\rm GHz}$ already found for 3CR/FRIs (Balmaverde et al. 2006), it is now attested for FR0s pointing towards a jet origin of both the radio and X-ray photons. As reported in Section 3.3, an intrinsic absorber is not required by the fit, at least for those sources having good quality X-ray spectra. Therefore, it is unlikely that the jet-related X-ray emission observed in FR0s is the unabsorbed component of a HEG-like spectrum. A similar result was obtained by Mingo et al. (2014), who concluded that the LEGs of their 2 Jy sample cannot be interpreted as simple heavily obscured HEGs (see also Baldi et al. 2010). This point is further strengthened below by the estimate of the Eddington-scaled luminosities for our FR0 sample.

From the stellar velocity dispersion relation of Tremaine et al. (2002)[15] we estimated the black hole masses ($M_{\rm BH}$) of our sample of FR0s. The values of $M_{\rm BH}$ range between $\sim 10^8$ and $\sim 10^9\,{\rm M}_\odot$ (see Table 4). From the relation $L_{\rm bol} = 3500\,L_{[\rm O\,III]}$ (Heckman et al. 2004) we derived the bolometric luminosities and successively the Eddington-scaled luminosities ($\dot{L} = L_{\rm bol}/L_{\rm Edd}$) given in Table 4. These estimates for the FR0s of our sample correspond to low values of $\dot{L}$ ($\sim 10^{-3}$–10^{-5}) typical of inefficient accretion modes [advection-dominated accretion flow (ADAF) like; Narayan & Yi 1994, 1995] and similar to those found for FRIs (see also Table B1) and for 2 Jy LEGs (Mingo et al. 2014).

This result strengthens the interpretation of a non-thermal origin of the high-energy nuclear emission in low-excitation compact sources, already suggested by the correlation between radio and X-ray emissions.

4.2 Compact radio galaxies versus BL Lac objects

The radio compactness of FR0s is due to the lack of extended emission and it is not related to a Doppler boosting of the jet radiation. This is evident in the compact radio galaxies that show emission lines with large equivalent widths in their optical spectra (such as Tol 1326−379; Grandi et al. 2016) but it is less straightforward in objects overwhelmed by the galaxy emission. Indeed, in this case, the stellar population dominates the emission hiding the nature of the underlying AGN that could be both a low-luminosity BL Lac with an extended jet pointed towards the observer, or a genuine compact radio galaxy.

In Fig. 1 it is evident that FR0s and low-luminosity BL Lacs occupy different regions of the $L_{[\rm O\,III]}$–$L_{1.4\,\rm GHz}$ plane. The two classes have similar emission-line luminosities but BL Lacs are more powerful in the radio band. This is expected since $L_{[\rm O\,III]}$ is an isotropic indicator of the AGN luminosity, while the radio emission suffers from relativistic effects.

The ratio between the [O III]λ5007 line and the 2–10 keV luminosities ($R_{[\rm O\,III]} = L_{[\rm O\,III]}/L_{(2-10\,\rm keV)}$) can be considered a useful tool to distinguish misaligned and aligned jets. We then collected [O III] luminosities of FRIs and FR0s from literature (Hardcastle et al. 2009; Leipski et al. 2009 ; Buttiglione et al. 2010, 2011) and from SDSS-DR7 survey,[16] respectively (see Appendix B and Table 4). For the [O III]-line luminosity of BL Lacs we refer to the work of Capetti & Raiteri (2015), while the X-ray 2–10 keV luminosity was directly obtained from the *Swift*/XRT instrument using the SSDC online data analysis tool.

The $R_{[\rm O\,III]}$ average values (including upper limits)[17] for FR0s and FRIs are consistent ($\langle R_{[\rm O\,III],\rm FR0}\rangle = -1.6 \pm 0.2$ and $\langle R_{[\rm O\,III],\rm FRI}\rangle = -1.7 \pm 0.2$). This is statistically attested by the TWOST test in ASURV (see Section 4.1 for details) that turns out with a probability $P_{\rm ASURV} = 0.9$. On the contrary, the Doppler boosting of the X-ray emission shifts the BL Lacs to lower values $\langle R_{[\rm O\,III],\rm BL\,Lacs}\rangle = -3.3 \pm 0.2$.

4.3 Compact radio galaxies versus young sources

The comparison between FR0s and young radio sources in the X-ray band suffers from the paucity of dedicated studies in this field (Kunert-Bajraszewska et al. 2014 and references therein). The samples of young sources for which high-energy information are available include mainly powerful GPS and CSS. These sources are generally different from ours being characterized by high X-ray (2–10 keV), radio (5 GHz), and [O III]-line luminosities typical of AGN with efficient accretion rates (Guainazzi et al. 2006; Vink et al. 2006; Labiano 2008; Siemiginowska et al. 2008; Tengstrand et al. 2009). Moreover, 16 CSO sources recently studied by Siemiginowska et al. (2016) in X-rays showed spectra generally flat and absorbed by intrinsic column densities (see also Ostorero et al. 2017).

Our sources seem more similar to three low-luminosity compact sources (LLC; Kunert-Bajraszewska & Thomasson 2009) discussed by Kunert-Bajraszewska et al. (2014) and classified as LEG. Their radio and X-ray luminosities (see table 2 of their work) locate these sources in our correlation strip shown in Fig. 4 (lower panel). The authors suggest that such LLC are intermittent radio sources rather than young objects evolving in FRIs, in line with the recent demographic study of Baldi et al. (2018a). They showed that the space density of FR0s in the local Universe ($z < 0.05$) is larger by a factor of $\sim$5 than FRIs, definitively rejecting the hypothesis that FR0s are young radio galaxies that will all eventually evolve into extended FRI radio sources.

5 SUMMARY AND CONCLUSIONS

We analysed 19 FR0s selected according to the criteria discussed in Section 2 and having public X-ray observations. Most of the sources have short exposures and/or large offsets. In spite of the limited quality of the data, our analysis allowed us to characterize for the first time FR0 sources at high energies.

FR0s have X-ray luminosities (2–10 keV) between 10^{40} and $10^{43}\,{\rm erg\,s^{-1}}$, comparable to FRIs. The clear correlation between radio and X-ray luminosities observed in both compact and extended objects, favours the interpretation of a non-thermal origin of the 2–10 keV photons. In agreement with FRIs, the high-energy

[14] The partial rank coefficient estimates the correlation coefficient between two variables after removing the effect of a third. If A and B are both related to the variable z, the partial Kendall's τ correlation coefficient is $\tau_{AB,z} = \frac{\tau_{AB}-\tau_{Az}\tau_{Bz}}{\sqrt{(1-\tau_{Az}^2)(1-\tau_{Bz}^2)}}$.

[15] $\log(M_{\rm BH}/{\rm M}_\odot) = (8.13 \pm 0.06) + (4.02 \pm 0.32)\log(\sigma/200\,{\rm km\,s^{-1}})$.

[16] http://classic.sdss.org/dr7/

[17] We used the Kaplan–Meier (KM) estimator in ASURV to derive the average values of $R_{[\rm O\,III]}$ in the presence of censored data.

Table 4. Radio, optical, and X-ray properties of the FR0 sample. (1) Identity number; (2) nuclear radio luminosity at 5 GHz; (3) X-ray nuclear luminosity (2–10 keV) corrected for absorption; (4) [O III] emission line luminosity, for all luminosities the proper k-correction was considered; (5) estimated black hole masses for the sources of the sample; and (6) Eddington-scaled luminosities ($\dot{L} = L_{\rm bol}/L_{\rm Edd}$).

Source name	$\log L_{5\,\rm GHz}$ (erg s^{-1})	$\log L_{\rm X,2-10\,keV}$ (erg s^{-1})	$\log L_{\rm [O\,III]}$[a] (erg s^{-1})	$\log M_{\rm BH}$ ($M_\odot$)	$\dot{L}$[b]
(1)	(2)	(3)	(4)	(5)	(6)
J004150.47−09	40.21	41.10	39.27	8.96	5.5×10^{-5}
J010101.12−00	39.52	<41.20	40.39	8.43	2.4×10^{-3}
J011515.78+00	39.97	41.15	39.51	8.57	2.3×10^{-4}
J015127.10−08	39.10	<40.49	39.29	7.97	5.6×10^{-4}
J080624.94+17	40.69	43.20	39.30	8.39	2.2×10^{-4}
J092405.30+14	41.38	42.16	40.68	9.06	1.1×10^{-3}
J093346.08+10	38.46	40.17	39.14	8.16	2.6×10^{-4}
J094319.15+36	40.25	40.94	39.81	7.89	2.2×10^{-3}
J104028.37+09	39.10	39.99	39.48	8.29	4.2×10^{-4}
J115954.66+30	39.71	<40.43	38.48	8.97	8.7×10^{-6}
J114232.84+26	40.91	42.14	40.24	8.51	1.4×10^{-3}
J122206.54+13	40.62	42.19	40.04	8.36	1.3×10^{-3}
J125431.43+26	39.93	42.02	39.61	8.59	2.8×10^{-4}
Tol 1326−379	39.79	42.29	40.60	8.30	5.0×10^{-3}
J135908.74+28	40.51	41.69	39.48	8.46	2.8×10^{-4}
J153901.66+35	40.82	42.20	40.07	8.31	1.5×10^{-3}
J160426.51+17	40.37	41.64	40.02	8.34	1.3×10^{-3}
J171522.97+57	39.46	<40.16	39.46	8.79	1.2×10^{-4}
J235744.10−00	39.30	40.93	40.26	8.76	8.5×10^{-4}

Notes. [a]Data are provided by the SDSS DR7 (http://www.sdss.org/).
[b]$\dot{L} = L_{\rm bol}/L_{\rm Edd}$. The bolometric luminosity is derived using the relation $L_{\rm bol} = 3500\,L_{\rm [O\,III]}$ measured by Heckman et al. (2004).

emission in FR0s is produced by the jet. Moreover, the high black hole masses (10^8–10^9 $M_\odot$) and the small values of the bolometric luminosities, as deduced from the [O III]-emission line, suggest an inefficient accretion process (ADAF like) at work also in the compact sources. These results confirm that the nuclear properties of FRIs and FR0s are similar and that the main difference between the two classes remains the lack of extended emission in FR0s.

We exclude important beaming effects in the X-ray spectra of FR0s on the basis of the ratio between the [O III] λ5007 line and the 2–10 keV luminosity ($R_{\rm [O\,III]}$). While the [O III]-line luminosity is expected to be emitted isotropically, the X-ray radiation could be amplified by Doppler boosting effects. While FR0s and FRIs have similar $R_{\rm [O\,III]}$ (~ -1.7), low-luminosity BL Lacs, whose X-ray radiation is beamed, have smaller values ($R_{\rm [O\,III]} \sim -3.3$).

A comparison with the X-ray properties of young sources is limited by the paucity of X-ray studies of GPS, CSS, and compact symmetric objects (CSO). Considering the available data, we do not find spectral similarities between these sources and FR0s. Generally, the studied young sources have higher X-ray luminosities (they are probably associated with an efficient accretion disc) and often show signatures of intrinsic absorption. Therefore, FR0s could be different sources characterized by intermittent activity, as in the case of J004150.47−09 and/or by jets with intrinsic properties that prevent the formation and evolution of extended structures.

ACKNOWLEDGEMENTS

The authors thank the anonymous referee for thoughtful comments that helped to improve the paper. ET acknowledges financial support from ASI-INAF grant 2015-023-R.O. This work is based on data from the *Chandra*, *XMM–Newton*, and *Swift* Data Archive. Part of this work is based on archival data, software, or online services provided by the ASI Science Data Center (ASDC). We thank the *Swift* team for making the ToO observation of Tol 1326−379 possible.

Funding for the SDSS and SDSS-II has been provided by the Alfred P. Sloan Foundation, the Participating Institutions, the National Science Foundation, the US Department of Energy, the National Aeronautics and Space Administration, the Japanese Monbukagakusho, the Max Planck Society, and the Higher Education Funding Council for England. The SDSS web site is http://www.sdss.org/.

REFERENCES

Ackermann M. et al., 2015, ApJ, 810, 14
Baldi R. D., Capetti A., 2008, A&A, 489, 989
Baldi R. D., Capetti A., 2009, A&A, 508, 603
Baldi R. D., Capetti A., 2010, A&A, 519, A48
Baldi R.D. et al., 2010, Apj, 725, 2426
Baldi R. D., Capetti A., Giovannini G., 2015, A&A, 576, A38 (B15)
Baldi R. D., Capetti A., Massaro F., 2018a, A&A, 609, A1
Baldi R. D. et al., 2018b, MNRAS, 476, 3478
Balmaverde B., Capetti A., 2006, A&A, 447, 97
Balmaverde B., Capetti A., 2015, A&A, 581, A76
Balmaverde B., Capetti A., Grandi P., 2006, A&A, 451, 35
Becker R. H., White R. L., Helfand D. J., 1995, ApJ, 450, 559
Bennett A. S., 1962, MNRAS, 125, 75
Best P. N., Heckman T. M., 2012, MNRAS, 421, 1569
Best P. N., Kauffmann G., Heckman T. M., Ivezić Ž., 2005, MNRAS, 362, 9
Bharadwaj V., Reiprich T. H., Lovisari L., Eckmiller H. J., 2015, A&A, 573, A75
Binette L., Magris C. G., Stasińska G., Bruzuel A. G., 1994, A&A, 292, 13
Bodo G., Mamatsashvili G., Rossi P., Mignone A., 2013, MNRAS, 434, 3030
Browne I. W. A. et al., 2003, MNRAS, 341, 13
Buttiglione S., Capetti A., Celotti A., Axon D. J., Chiaberge M., Macchetto F. D., Sparks W. B., 2009, A&A, 495, 1033
Buttiglione S., Capetti A., Celotti A., Axon D. J., Chiaberge M., Macchetto F. D., Sparks W. B., 2010, A&A, 509, A6
Buttiglione S., Capetti A., Celotti A., Axon D. J., Chiaberge M., Macchetto F. D., Sparks W. B., 2011, A&A, 525, A28

Cao W., Rawlings S., 2004, MNRAS, 349, 1419
Capetti A., Baldi R. D., 2011, A&A, 529, A126
Capetti A., Raiteri C. M., 2015, A&A, 580, A73
Capetti A., Massaro F., Baldi R. D., 2017, A&A, 598, A49
Colbert J. W., Mulchaey J. S., Zabludoff A., 2001, AJ, 121, 808
Colla G., Fanti C., Fanti R., Gioia I., Lari C., Lequeux J., Lucas R., Ulrich M.-H., 1975, A&A, 38, 209
Condon J. J., Cotton W. D., Greisen E. W., Yin Q. F., Perley R. A., Taylor G. B., Broderick J. J., 1998, AJ, 115, 1693
Dasadia S. et al., 2016, MNRAS, 458, 681
de Vaucouleurs G., de Vaucouleurs A., Corwin H. G., Jr, 1976, Second Reference Catalogue of Bright Galaxies. University of Texas Press, Austin, TX
Díaz-Giménez E., Mamon G. A., Pacheco M., Mendes de Oliveira C., Alonso M. V., 2012, MNRAS, 426, 296
Dressler A., 1980, ApJS, 42, 565
Edge D. O., Shakeshaft J. R., McAdam W. B., Baldwin J. E., Archer S., 1959, Mem. R. Astron. Soc., 68, 37
Fabbiano G., Kim D. W., Trinchieri G., 1992, ApJS, 80, 531
Fanaroff B. L., Riley J. A., 1974, MNRAS, 167, 31
Fanti R., Gioia I., Lari C., Ulrich M. H., 1978, A&AS, 34, 341
Feigelson E. D., Nelson P. I., 1985, ApJ, 293, 192
Feretti L., Giovannini G., 1994, A&A, 281, 375
Ghisellini G., 2011, in Aharonian F. A., Hofmann W., Rieger F. M., eds, AIP Conf. Proc. Vol. 1381, 25th Texas Symposium on Relativistic Astrophysics (Texas 2010). Am. Inst. Phys., New York, p. 180
Giovannini G., Feretti L., Gregorini L., Parma P., 1988, A&A, 199, 73
Giovannini G., Cotton W. D., Feretti L., Lara L., Venturi T., 2001, ApJ, 552, 508
Graham A. W., Erwin P., Caon N., Trujillo I., 2001, ApJ, 563, 11
Grandi P., Capetti A., Baldi R. D., 2016, MNRAS, 457, 2
Guainazzi M., Siemiginowska A., Stanghellini C., Grandi P., Piconcelli E., Azubike Ugwoke C., 2006, A&A, 446, 87
Hardcastle M. J., Evans D. A., Croston J. H., 2009, MNRAS, 396, 1929
Heckman T. M., Kauffmann G., Brinchmann J., Charlot S., Tremonti C., White S. D. M., 2004, ApJ, 613, 109
Helfand D. J., White R. L., Becker R. H., 2015, ApJ, 801, 26
Hlavacek-Larrondo J., Fabian A. C., Edge A. C., Ebeling H., Allen S. W., Sanders J. S., Taylor G. B., 2013, MNRAS, 431, 1638
Isobe T., Feigelson E. D., Nelson P. I., 1986, ApJ, 306, 490
Jackson N., Rawlings S., 1997, MNRAS, 286, 241
Kalberla P. M. W., Burton W. B., Hartmann D., Arnal E. M., Bajaja E., Morras R., Pöppel W. G. L., 2005, A&A, 440, 775
Kewley L. J., Groves B., Kauffmann G., Heckman T., 2006, MNRAS, 372, 961
Koester B. P. et al., 2007, ApJ, 660, 239
Kunert-Bajraszewska M., Thomasson P., 2009, Astron. Nachr., 330, 210
Kunert-Bajraszewska M., Labiano A., Siemiginowska A., Guainazzi M., 2014, MNRAS, 437, 3063
Labiano A., 2008, A&A, 488, L59
Laing R. A., Jenkins C. R., Wall J. V., Unger S. W., 1994, in Bicknell G. V., Dopita M. A., Quinn P. J., eds, ASP Conf. Ser. Vol. 54, The First Stromlo Symposium: The Physics of Active Galaxies. Astron. Soc. Pac., San Francisco, p. 201
Lanz L., Ogle P. M., Evans D., Appleton P. N., Guillard P., Emonts B., 2015, ApJ, 801, 17
Leipski C., Antonucci R., Ogle P., Whysong D., 2009, ApJ, 701, 891
Marchesini D., Celotti A., Ferrarese L., 2004, MNRAS, 351, 733
Massaro F. et al., 2010, ApJ, 714, 589
Massaro F. et al., 2012, ApJS, 203, 31
Massaro F., Harris D. E., Tremblay G. R., Liuzzo E., Bonafede A., Paggi A., 2013, ApJS, 206, 7
Mezcua M., Prieto M. A., 2014, ApJ, 787, 62
Migliori G. et al., 2011, A&A, 533, A72
Mingo B., Hardcastle M. J., Croston J. H., Dicken D., Evans D. A., Morganti R., Tadhunter C., 2014, MNRAS, 440, 269
Mingo B. et al., 2016, MNRAS, 462, 2631
Murphy T. et al., 2010, MNRAS, 402, 2403
Myers S. T. et al., 2003, MNRAS, 341, 1
Nagar N. M., Falcke H., Wilson A. S., 2005, A&A, 435, 521
Narayan R., Yi I., 1994, ApJ, 428, 13
Narayan R., Yi I., 1995, ApJ, 444, 231
Ogle P., Boulanger F., Guillard P., Evans D. A., Antonucci R., Appleton P. N., Nesvadba N., Leipski C., 2010, ApJ, 724, 1193
Ostorero L., Morganti R., Diaferio A., Siemiginowska A., Stawarz Ł., Moderski R., Labiano A., 2017, ApJ, 849, 34
Owen F. N., Ledlow M. J., Keel W. C., 1995, AJ, 109, 14
Pandge M. B., Vagshette N. D., David L. P., Patil M. K., 2012, MNRAS, 421, 808
Pilkington J. D. H., Scott J. F., 1965, Mem. R. Astron. Soc., 69, 183
Prada F. et al., 2003, ApJ, 598, 260
Rosen S. R. et al., 2016, A&A, 590, A1
Sadler E. M., 2016, Astron. Nachr., 337, 105
Sadler E. M., Ekers R. D., Mahony E. K., Mauch T., Murphy T., 2014, MNRAS, 438, 796
Sarzi M. et al., 2010, MNRAS, 402, 2187
Siemiginowska A., LaMassa S., Aldcroft T. L., Bechtold J., Elvis M., 2008, ApJ, 684, 811
Siemiginowska A., Sobolewska M., Migliori G., Guainazzi M., Hardcastle M., Ostorero L., Stawarz L., 2016, ApJ, 823, 57
Spergel D. N. et al., 2007, ApJS, 170, 377
Tengstrand O., Guainazzi M., Siemiginowska A., Fonseca Bonilla N., Labiano A., Worrall D. M., Grandi P., Piconcelli E., 2009, A&A, 501, 89
Tremaine S. et al., 2002, ApJ, 574, 740
Trichas M. et al., 2013, ApJ, 778, 188
Ulvestad J. S., Ho L. C., 2001, ApJ, 558, 561
Vink J., Snellen I., Mack K.-H., Schilizzi R., 2006, MNRAS, 367, 928
Woo J.-H., Urry M. C., 2002, ApJ, 579, 530
Yang Y., Huo Z., Zhou X., Xue S., Mao S., Ma J., Chen J., 2004, ApJ, 614, 692
York D. G. et al., 2000, AJ, 120, 1579

APPENDIX A: NOTES AND ANALYSIS DETAILS ON INDIVIDUAL SOURCES

In the following, notes on individual FR0 sources are provided, while the details of the X-ray data reduction are presented in Table A1.

A1 J004150.47−09

At the centre of the cluster Abell 85. This cluster presents X-ray cavities created by the central AGN, as it is evident from the *Chandra* 3–7 keV image (Hlavacek-Larrondo et al. 2013). The presence of such cavities suggests that this AGN produced in the past an extended radio source able to excavate the external medium; this is an indication of recurrency.

A2 J010101.12−00

This source is part of the B15 sample (their ID590) observed with the Karl G. Jansky Very Large Array (JVLA). For this object we could only obtain an upper limit on the 2–10 keV flux estimated from the *Chandra* count rate using WEBPIMMS and assuming a spectral slope $\Gamma = 2$.

A3 J011515.78+00

This source, GIN 061, is part of the sample of FR0s presented in B15 (their ID605). It lies at the outskirts of the Abell cluster A168 (Dressler 1980), as shown by the *Chandra* (Yang et al. 2004) and *XMM–Newton* (Fig. 3) X-ray images. The good quality of the

Table A1. Details of the data reduction for the sample of FR0s.

Source (Instr.)	Reg.	Shape[a]	R^b (arcsec)	$R_{in}{}^c$ (arcsec)	$R_{out}{}^d$ (arcsec)	X-ray cluster[e]
J004150.47−09	s	c	2.8	–	–	Yes
(*Chandra*)	b	a	–	5.5	7.8	
J010101.12−00	s	c	5	–	–	?
(*Chandra*)	b	a	–	7.1	9.6	
J011515.78+00	s	c	16	–	–	Yes
(*XMM*)	b	c	16	–	–	
J015127.10−08	s	c	20	–	–	?
(*Swift*)	b	a	–	40	80	
J080624.94+17	s	c	20	–	–	?
(*Swift*)	b	a	–	40	80	
J092405.30+14	s	c	2.5	–	–	Yes
(*Chandra*)	b	a	–	3.8	5.4	
J093346.08+10	s	c	20	–	–	?
(*Swift*)	b	a	–	40	80	
J094319.15+36	s	c	20	–	–	?
(*Swift*)	b	a	–	40	80	
J104028.37+09	s	c	22	–	–	No
(*XMM*)	b	c	22	–	–	
J114232.84+26	s	c	26.5	–	–	?
(*XMM*)	b	a	–	57.4	87.7	
J115954.66+30	s	c	20	–	–	?
(*Swift*)	b	a	–	40	80	
J122206.54+13	s	c	20	–	–	?
(*Swift*)	b	a	–	40	80	
J125431.43+26	s	c	2.7	–	–	No
(*Chandra*)	b	a	–	4.5	8.8	
Tol 1326−379	s	c	20	–	–	No
(*Swift*)	b	a	–	40	80	
J135908.74+28	s	c	4.5	–	–	Yes
(*Chandra*)	b	a	–	8.1	16.7	
J153901.66+35	s	c	20	–	–	?
(*Swift*)	b	a	–	40	80	
J160426.51+17	s	c	6.6	–	–	Yes
(*Chandra*)	b	a	–	8.7	14.5	
J171522.97+57	s	c	3.3	–	–	Yes
(*Chandra*)	b	a	–	4.7	9.5	
J235744.10−00[f]	–	–	–	–	–	?

Notes. [a]Shape of the extraction region: c – circle; a – annulus.
[b]Radius of the circular region.
[c]Internal radius of the annular region.
[d]External radius of the annular region.
[e]The source is within (or at the edge of) a cluster or a group of galaxies in the X-ray image.
[f]The source is part of the 3*XMM*-DR6 catalogue of serendipitous sources (Rosen et al. 2016).

XMM–Newton spectrum allowed us to constrain the parameters of the power law ($\Gamma = 2.0 \pm 0.2$) and the thermal component ($kT = 0.8 \pm 0.1$).

A4 J015127.10−08

The X-ray spectrum of this source (also known as NGC 0707) can be reproduced by a power law plus a thermal model with $kT \sim 0.2$ keV. This latter component is dominant, and for the power law we could estimate only an upper limit on the 2–10 keV flux.

A5 J080624.94+17

From the work of Koester et al. (2007) the source seems to reside in a galaxy cluster. However, the statistics of the X-ray data is too low to constrain the parameters of a thermal component. Therefore the spectrum is fitted with an absorbed power-law fixing $\Gamma = 2$.

A6 J092405.30+14

The source resides close to the centre of the cluster Abell 795. The X-ray spectrum can be well reproduced by a power law with $\Gamma = 1.8$ plus an APEC component with $kT = 1.3$ keV related to the thermal gas of cluster.

A7 J093346.08+10

In NGC 2911 an extended jet radio emission on subarcsecond scales has been observed (Mezcua & Prieto 2014), meaning that this source is powerful enough to launch radio jets, at least on pc scales.

A8 J094319.15+36

NGC 2965. The *Swift* spectrum of this source can be modelled with a steep power law ($\Gamma = 2.3$) only absorbed by Galactic column density. However, the low statistics prevented us from establishing the presence of a possible thermal component.

A9 J104028.37+09

NGC 3332 resides in an isolated elliptical galaxy (Colbert et al. 2001). Its X-ray spectrum can be reproduced by a steep ($\Gamma = 2.2 \pm 0.4$) power law absorbed only by the Galactic column density.

A10 J114232.84+26

NGC 3826 is a member of a compact group of galaxies included in the photometric catalogue of Díaz-Giménez et al. (2012). The source lies at the edge of the *XMM–Newton*/PN field of view (offset = 13.7 arcmin) since the main target was the star GJ 436. In spite of the poor statistics, the spectrum is better fitted with two components: a thermal model, probably related to the intracluster medium (ICM), and a power law emerging above 2 keV. When the spectral slope, initially fixed to $\Gamma = 2$, was let free to vary it assumed a smaller value suggesting the presence of intrinsic absorption. We could not constrain the value of the intrinsic N_H but providing an upper limit on this parameter $N_H < 3.4 \times 10^{23}$ cm^{-2}.

A11 J115954.66+30

This source at $z = 0.106$ is among the three farthest objects of the sample. We do not have any information about the environment either from the *Swift* X-ray image or from the literature. We reproduced the XRT spectrum with a power law fixing the photon index to $\Gamma = 2$.

A12 J122206.54+13

The source is also known with the name VPC 0184 and is associated with the cluster Abell 1526, which however is not visible in our *Swift*/XRT image. The X-ray spectrum can be reproduced by a power law with photon index fixed to a value of 2. Indeed, the statistics is good enough neither to constrain this parameter nor to

establish the possible presence of thermal gas related to the cluster. For this reason we are aware that the X-ray flux that we report in Table 3 could be overestimated.

A13 J125431.43+26

This source is already present in the *Chandra* Source Catalog to Sloan Digital Sky Survey (CSC/SDSS) sample by Trichas et al. (2013). The X-ray spectral parameters presented in this paper are in agreement with those found by Trichas et al. We have no information on the environment either from the X-ray image or from the literature.

A14 Tol 1326−379

Tol 1326−379 is a FR0 source at $z = 0.0284$ hosted in an early-type galaxy. It is the first FR0 with an associated γ-ray counterpart (Grandi et al. 2016). Indeed, it is listed in the Third LAT AGN Catalog (3LAC) as 3FGL J1330.0−3818 (Ackermann et al. 2015). As it is evident from Table 3 the photon index of this γ-ray FR0 is quite flat $\Gamma = 1.3 \pm 0.4$. However, the inclusion of an intrinsic absorber did not significantly improve the fit. We could only estimate an upper limit to the intrinsic column density $N_{\rm H} < 3.4 \times 10^{22}\,{\rm cm}^{-2}$.

A15 J135908.74+28

This source, Zw 162−39, resides in the Abell cluster A1831 (Feretti & Giovannini 1994), as it shown in Fig. 3. Indeed, the residuals in the X-ray spectrum suggest the presence of a thermal component in addition to the power law. The estimated best-fitting value of the gas temperature is $kT = 0.24$ keV.

A16 J153901.66+35

The very low statistics of the X-ray spectrum prevents us from establishing the presence of diffuse emission around the source. Therefore the spectrum is fitted with an absorbed power law fixing $\Gamma = 2$.

A17 J160426.51+17

This source, NGC 6040B, lies at the outskirts of the cluster Abell 2151 (also known as Hercules cluster). Together with NGC 6040A, located at 0.5 arcmin, it forms an interacting pair (de Vaucoulers, de Vaucoulers & Corwin 1976). The X-ray spectrum is well reproduced by an absorbed power law. The flatness of the photon index ($\Gamma = 1.1$, see Table 3) suggests the possible presence of extra absorption. However, the low statistics prevent us from constraining the value of this additional component, for which we could only estimate an upper limit $N_{\rm H} < 4.9 \times 10^{22}\,{\rm cm}^{-2}$.

A18 J171522.97+57

NGC 6338 is part of a cool-core cluster (Bharadwaj et al. 2015). The X-ray spectrum is dominated by the thermal component of the cluster, for which we could constrain also the abundances to a value of 0.3. The power law is marginally significant in fact we could only determine an upper limit to the flux of this component.

A19 J235744.10−00

The X-ray flux of this source, which is part of the B15 sample (their ID535), is provided by the 3*XMM*-DR6 catalogue (Rosen et al. 2016). Prada et al. (2003) list this source as an isolated galaxy.

APPENDIX B: FRI

Radio, optical, and X-ray data of the 35 3CR–3CRR/FRIs in Table B1 are from Buttiglione et al. (2009, 2010, 2011), Leipski et al. (2009), Lanz et al. (2015), Balmaverde et al. (2006), Hardcastle et al. (2009), Ogle et al. (2010), Migliori et al. (2011), Mingo et al. (2014), and Dasadia et al. (2016).

For 11 sources the X-ray luminosities were obtained directly analysing *Chandra* data using the software CIAO (v.4.7) and calibration data base v.4.6.9. We followed standard procedures to extract source and background spectra. For the source we chose a circular region varying between 2.5 and 7 arcsec. Only in two cases, e.g. 3C 371 and 3C 465, data were strongly piled up and therefore the spectra were extracted from annular regions ($r_{\rm in} = 0.5$ arcsec, $r_{\rm out} = 2.5$ arcsec). All background spectra were taken from annular regions with $r_{\rm in}$ and $r_{\rm out}$ ranging between 3–16 and 4–30 arcsec, respectively. Data were then grouped to a minimum of 15 counts bin^{-1} over the energy range 0.5–7 keV. This allows us to apply the χ^2 statistics. For 3C 29, 3C 76.1, and 3C 129 data were not grouped and the C-statistics was applied. As a baseline model we adopted a power law absorbed by Galactic column density. The photon index was let free to vary except for 3C 310 and 3C 424: in these cases Γ was fixed to 2. When the residuals were not satisfactory a thermal component was added to the data. Finally, in case the value of the photon index was very flat, we included an intrinsic $N_{\rm H}$ to the model. The results of the spectral analysis are summarized in Table B2.

Table B1. Multiwavelength properties of the comparison sample of FRIs: (1) name; (2) redshift; (3) radio core luminosity at 5 GHz; (4) X-ray (2–10 keV) luminosity; (5) [O III] emission line luminosity; (6) NVSS 1.4 GHz radio luminosity; (7) black hole masses from Marchesini, Celotti & Ferrarese (2004), Woo & Urry (2002), Graham et al. (2001), and Cao & Rawlings (2004); (8) Eddington-scaled luminosities ($\dot{L}$); and (9) references for the X-ray luminosities. For all luminosities the proper *k*-correction was considered.

Name	z	$\log L_{(5\,\mathrm{GHz})}$	$\log L_{(2-10\,\mathrm{keV})}$	$\log L_{[\mathrm{O\,III}]}$	$\log L_{(1.4\,\mathrm{GHz})}$	M_{BH}	$\dot{L}^a$	Ref.
3C 29	0.0448	40.33	41.38	40.09	41.32	8.81	5.1×10^{-4}	2
3C 31	0.0169	39.4	40.73	39.46	39.90	7.89	1.0×10^{-3}	1
3C 66B	0.0215	39.9	41.17	40.05	40.32	8.84	4.4×10^{-4}	1
3C 75	0.0232	39.3	<41.11	<39.92	37.86	9.0	$<2.2 \times 10^{-4}$	1
3C 76.1	0.0324	39.07	40.92	39.85	40.74	8.13	1.4×10^{-3}	2
3C 78	0.0288	40.88	42.37	39.41	41.17	8.98	7.2×10^{-5}	1
3C 83.1	0.0251	39.11	41.2	<39.5	40.40	9.01	$<8.3 \times 10^{-5}$	1
3C 84	0.0176	42.08	42.7	41.6	41.33	9.28	5.6×10^{-3}	1
3C 89	0.138	41.08	41.77	40.51	42.09	8.83	1.3×10^{-3}	5
3C 129	0.0208	39.21	40.11	<39.85	40.74	–	–	2
3C 130	0.109	40.64	41.57	–	41.62	–	–	2
3C 189	0.043	40.53	41.94	39.94	41.20	8.93	2.7×10^{-4}	1
3C 264	0.0217	39.98	41.87	39.2	40.71	8.85	6.0×10^{-5}	3
3C 270	0.0074	39.2	40.73	38.96	39.83	8.57	6.6×10^{-5}	1
3C 272.1	0.0037	38.36	39.51	38.2	39.12	8.35	1.9×10^{-5}	1
3C 274	0.0037	39.72	40.35	38.99	40.76	8.26	1.4×10^{-4}	1
3C 293	0.0452	40.36	42.78	39.8	41.42	7.99	1.7×10^{-3}	3
3C 296	0.0237	39.61	41.38	39.78	40.39	9.13	1.2×10^{-4}	1
3C 310	0.053	40.41	<40.41	40.05	41.86	8.29	1.5×10^{-3}	2
3C 315	0.1083	41.34	41.68	40.86	42.17	8.7	3.9×10^{-3}	4
3C 317	0.0342	40.64	41.44	40.35	41.30	8.80	9.5×10^{-4}	1
3C 338	0.0303	39.96	<40.76	39.57	41.02	9.23	5.9×10^{-5}	1
3C 346	0.162	41.74	43.45	41.32	42.53	8.89	7.2×10^{-3}	1
3C 348	0.154	40.36	<42.69	40.4	41.85	8.84	9.8×10^{-4}	1
3C 371	0.05	41.55	42.89	40.94	41.17	–	–	2
3C 386	0.017	38.65	39.75	40.2	40.62	8.5	1.3×10^{-3}	4
3C 402	0.0259	39.48	41.20	<39.42	40.60	8.18	$<4.7 \times 10^{-4}$	2
3C 424	0.126	40.56	42.57	40.80	42.15	8.17	1.1×10^{-2}	2
3C 438	0.29	41.15	<43.14	41.46	43.01	8.80	1.2×10^{-2}	3
3C 442	0.0263	38.19	41.17	39.21	40.22	8.28	2.3×10^{-4}	2
3C 449	0.0181	39.04	<40.46	39.19	39.32	7.71	8.1×10^{-4}	1
3C 465	0.0303	40.44	40.60	39.81	40.43	9.32	8.3×10^{-5}	2
NGC 6109	0.0296	39.44	40.06	–	40.01	–	–	3
NGC 6251	0.024	40.35	42.76	39.86	40.15	8.77	3.3×10^{-4}	6
NGC 7385	0.026	39.90	41.07	–	40.41	–	–	2

Notes. [a] $\dot{L} = L_{\mathrm{bol}}/L_{\mathrm{Edd}}$. The bolometric luminosity is derived from the relation $L_{\mathrm{bol}} = 3500\,L_{[\mathrm{O\,III}]}$ (Heckman et al. 2004) as for FR0s (see Table 4).
References: 1 - Balmaverde et al. (2006); 2 - this work; 3 - Hardcastle et al. (2009); 4 - Ogle et al. (2010); 5 - Dasadia et al. (2016); 6 - Migliori et al. (2011).

Table B2. Spectral results for the 11 FRIs analysed with *Chandra*.

Name	$N_{\mathrm{H,Gal}}$ (cm^{-2})	$N_{\mathrm{H,int}}$ (cm^{-2})	Γ	kT (keV)	$F_{\mathrm{th},0.5-5\,\mathrm{keV}}$ ($\mathrm{erg\,cm^{-2}\,s^{-1}}$)	$F_{\mathrm{nucl},2-10\,\mathrm{keV}}$ ($\mathrm{erg\,cm^{-2}\,s^{-1}}$)
3C 29	3.7×10^{20}	$<0.2 \times 10^{23}$	2.4 ± 0.5	–	–	$(5.0^{+2.5}_{-1.7}) \times 10^{-14}$
3C 76.1	9.5×10^{20}	–	$1.9^{+1.2}_{-0.9}$	–	–	$(1.5^{+0.9}_{-0.6}) \times 10^{-14}$
3C 129	5.9×10^{21}	–	$2.3^{+0.8}_{-0.7}$	–	–	$(1.3^{+0.9}_{-0.6}) \times 10^{-14}$
3C 130	3.7×10^{21}	–	1.9 ± 0.4	–	–	$(2.4 \pm 0.7) \times 10^{-14}$
3C 310	3.7×10^{20}	–	2.0 (f)	$1.2^{+0.2}_{-0.5}$	$(6.4^{+4.1}_{-4.3}) \times 10^{-15}$	$<2.4 \times 10^{-15}$
3C 371	4.2×10^{20}	–	1.3 ± 0.06	$0.3^{+0.2}_{-0.1}$	$(2.7^{+1.8}_{-1.7}) \times 10^{-14}$	$(1.4 \pm 0.1) \times 10^{-12}$
3C 402	1.1×10^{21}	–	2.1 ± 0.4	–	–	$(1.0 \pm 0.2) \times 10^{-13}$
3C 424	7.0×10^{20}	–	2.0 (f)	–	–	$(8.6^{+2.4}_{-2.0}) \times 10^{-14}$
3C 442	4.9×10^{20}	$(0.9 \pm 0.3) \times 10^{22}$	1.9 ± 0.3	–	–	$(9.9^{+20.1}_{-6.2}) \times 10^{-14}$
3C 465	1.9×10^{21}	–	$1.7^{+0.8}_{-1.1}$	0.9 ± 0.05	$(8.6^{+1.3}_{-1.4}) \times 10^{-14}$	$(2.2^{+2.5}_{-1.6}) \times 10^{-14}$
NGC 7385	1.6×10^{21}	–	2.6 ± 0.3	–	–	$(7.6^{+2.1}_{-1.6}) \times 10^{-14}$

This paper has been typeset from a TEX/LATEX file prepared by the author.